Acta Radiologica Open
7(5) 1–13

DOI: 10.1177/2058460118776487
journals.sagepub.com/home/arr
SAGE

Imaging review of the anterior skull base

Olivia Francies[1], Levan Makalanda[1], Dimitris Paraskevopolous[2] and Ashok Adams[1]

Abstract

The anterior skull base (ASB) is intimately associated with the unique soft tissue subtypes of the nasal cavity, paranasal sinuses, orbits, and intracranial compartment. Pathology involving the ASB is rare but the causes are manifold and can be broadly subdivided into those intrinsic to the skull base and processes extending from below or above. Sinonasal pathology is the most commonly encountered and poses significant management challenges that rely heavily on accurate interpretation of the radiological findings. We illustrate the normal anatomy of the ASB and present a cross-sectional imaging review of the pathological entities that may be encountered, focusing on the specific features that will impact on clinical and surgical management.

Keywords

Paranasal sinuses, anterior skull base, sinonasal carcinoma, CT, MRI, anatomy

Date received: 24 August 2017; accepted: 17 April 2018

Introduction

The skull base is divided into compartments corresponding to the division of the brain into anterior, middle, and posterior cranial fossae. The anterior skull base (ASB) is formed laterally by the orbital plates of the frontal bone, medially by the cribriform plate and crista galli of the ethmoid bone, and posteriorly by the planum sphenoidale and lesser wings of the sphenoid bone (Figs. 1 and 2). The olfactory nerves, which pass from the nasal epithelium through the cribriform plate, can be involved by pathology affecting the ASB, as can the optic nerve canals, which open into the middle cranial fossa between the lesser and greater sphenoid wings.

Pathology affecting the ASB can be broadly subdivided into intrinsic skull base causes and processes that extend from above (intracranial compartment) or from below (nasal cavity, paranasal sinuses, and orbits). Pathological processes extending superiorly from the sinonasal region are the most common, in part due to the thin barrier of the cribriform plate, and range from benign entities, e.g. mucocele, to the more aggressive infectious and neoplastic processes, e.g. squamous cell carcinoma (SCC). Abnormalities extending from above and those intrinsic to the ASB are much less commonly encountered but include congenital conditions, e.g. fibrous dysplasia (FD), and acquired benign and malignant pathologies, e.g. cerebrospinal fluid (CSF) leak, skull base metastases.

Computed tomography (CT) and magnetic resonance imaging (MRI) with multi-planar reconstructions are essential in the investigation, diagnosis, and management of ASB pathology. A comprehensive knowledge of the anatomy in this area is crucial for accurate interpretation and delineation of pathology. The aim of this pictorial review is to present a variety of ASB pathology, focusing on the pertinent imaging features that may affect the management of these patients for surgeons, oncologists, and interventional radiologists.

[1]Department of Radiology, St Bartholomew's and The Royal London Hospitals, Barts Health NHS Trust, London, UK
[2]Department of Neurosurgery, The Royal London Hospital, Barts Health NHS Trust, London UK

Corresponding author:
Ashok Adams, Imaging Department, Barts Health NHS Trust, Whitechapel Road, London E1 1BB, UK.
Email: ashok.adams@bartshealth.nhs.uk

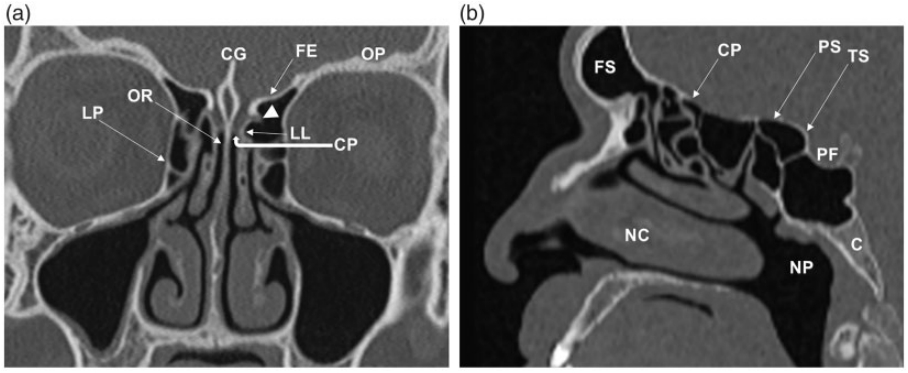

Fig. 1. Coronal (a) and para-midline sagittal (b) CT images of the normal anatomy of the ASB (in different patients). The crista galli (CG), cribriform plate (CP), and lateral lamella (LL) form the olfactory fossa. The anterior ethmoidal artery enters the olfactory fossa through the LL (arrowhead). The fovea ethmoidalis (FE)/roof of the ethmoid labyrinth is continuous with the orbital plate (OP) of the frontal bone. The olfactory niche or recess (OR) is located between the perpendicular plate of the nasal septum and the vertical insertion of the middle turbinate. The intimate relationship between the ASB, nasal cavity (NC), paranasal sinuses, orbits, middle skull base, and nasopharynx (NP) can be appreciated.
LP, lamina papyracea; FS, frontal sinus; PS, planum sphenoidale; TS, tuberculum sella of the sphenoid bone; PF, pituitary fossa; C, clivus.

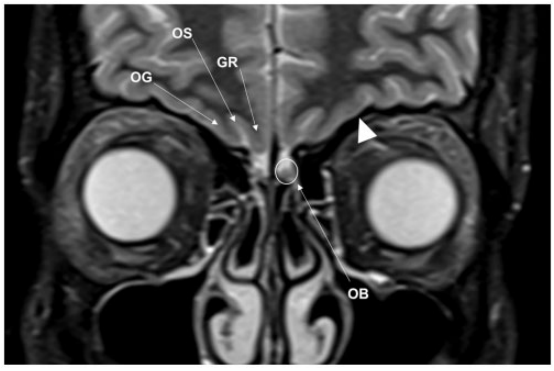

Fig. 2. Normal inferior frontal lobe anatomy related to the ASB on MRI. This coronal STIR image demonstrates the olfactory bulb (OB) lying on the cribriform plate within the olfactory fossa. OB signal is isointense to gray matter. Components of the inferior frontal lobe include the gyrus rectus (GR), olfactory sulcus (OS) and the medial orbital gyrus (OG). Note the normal low T2W signal of cortical bone (arrowhead).

Imaging the anterior skull base

CT and MRI are often used in conjunction; axial section thickness should be kept to a minimum and coronal imaging is mandatory. CT is usually the first-line modality, allowing delineation of soft tissue abnormality as well as evaluating for bone remodeling or destruction. Signs of the latter can indicate whether pathology is slow-growing and more likely benign, or aggressive and fast-growing. CT imaging is a prerequisite for endoscopic and open surgical planning of any ASB abnormality. In this regard, the depth of the olfactory fossa, determined by the height of the lateral lamella, is important to note in order to prevent potential complications from functional endoscopic sinus surgery (FESS) (Fig. 1). It is measured according to the Keros classification, with the greater the height having the higher risk of anterior cranial fossa penetration: 1–3 mm in type I; 4–7 mm in type II (commonest); and 8–16 mm in type III (1,2). Knowledge of the location of the anterior ethmoidal foramen, wherein lies the anterior ethmoidal artery (Fig. 1), is important as this structure is also at risk of injury during FESS. In our institution we use high-resolution 0.75-mm section thickness, in contiguous increments with tri-planar reconstructions in bone and soft tissue reformats. Due to the inherent rarity of the cribriform plate (range = 0.05–0.2 mm (1)), even with the use of high-resolution CT imaging, assessment of its integrity in specific clinical settings, e.g. CSF leak, will be limited. The use of intravenous iodinated contrast material is dependent on the clinical question.

MRI is indicated for suspected involvement of the intracranial compartment, equivocal involvement of the ASB on CT, and for delineation of tumor from obstructed secretions within the sinonasal region. Our standard craniofacial MRI protocol includes coronal and axial T1-weighted (T1W) and T2-weighted (T2W) sequences, post-contrast T1W, including fat-saturated sequences (we use the short tau inversion recovery [STIR] technique), and diffusion-weighted imaging (DWI). A steady state gradient echo sequence, such as constructive interference in steady state (CISS), can provide better contrast between CSF and the orbitofrontal region than conventional T2W imaging (3). The overall field of view (FOV) should include the clavicles, in order to assess cervical lymph nodes, but high-resolution, small FOV images should be centered on the site of pathology, e.g. sinonasal region.

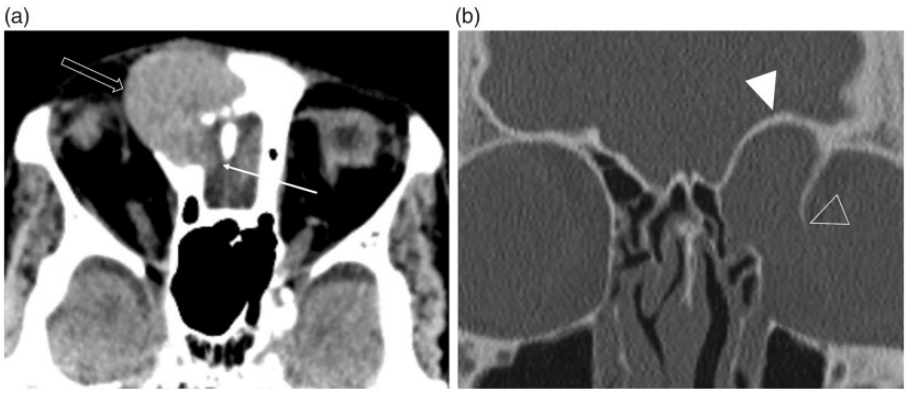

Fig. 3. Intracranial and orbital extension of a fronto-ethmoidal mucocele (in different patients). (a) The axial non-contrast CT image in soft tissue windowing demonstrates a well-defined hyperdense lesion arising in the region of the right frontal sinus drainage pathway. This has eroded through the cribriform plate and postero-inferior wall of the frontal sinus (arrow), with extension into the anterior cranial fossa, as well as the lamina papyracea anteriorly (open arrow). It is important to note that the adjacent low attenuation orbital fat has normal appearances, i.e. there is no evidence of an infiltrative or aggressive soft tissue disease process. (b) The coronal image in bone windowing demonstrates the expansile remodeling of the ASB (arrowhead) and smooth erosion with complete dehiscence of the left lamina papyracea (open arrowhead) indicating a long-standing (benign) pathology.

Post-intravenous gadolinium MRI plays an important role in ASB imaging, e.g. delineating enhancing tumor from retained secretions in the sinonasal cavities, and intracranially, helping to distinguish between dural hyperemia (smooth and linear) and dural invasion (>5 mm thickening or nodular) in patients with sinonasal malignancy with intracranial extension (4,5). The T1W and T1W post-contrast fat-suppressed sequences are particularly useful for depicting bone marrow and orbital fat invasion by tumor or infection, which replace the normal bright signal of fat. The low signal T2W line representing the periorbita or cortical bone at the ASB must be closely interrogated for any discontinuity indicating a potential site of dehiscence or invasion (Fig. 2). DWI is particularly helpful in the assessment of intracranial spread of infection and differentiating tumor from inflammatory or post-treatment change (6).

Lesions affecting the ASB from below

Benign conditions

Imaging requests of the nasal cavity and paranasal sinuses are common, usually to evaluate polyps and rhinosinusitis before FESS, and non-contrast CT is the usual first-line modality. Despite nasal polyps having an estimated prevalence of 4% in the general population, polyposis resulting in ASB dehiscence is extremely rare and should not routinely be considered as a differential in ASB pathology (7,8). These scans should be evaluated for the presence of secondary mucocele formation, which occurs from obstruction of a sinus drainage pathway (9). These are most common within the frontal sinuses (60–65%) and, although benign, they can expand concentrically causing pressure-erosion of surrounding bones with orbital and/or intracranial extension occurring when gradual bone remodeling results in complete dehiscence (Fig. 3) (10,11) These mucoid-filled cavities demonstrate differing CT densities and MR signal characteristics depending on the protein:water ratio (9). Compression of neurovascular structures from mass effect and superadded infection are important reasons for prompt management (2).

Contrast-enhanced CT imaging is indicated in complicated cases of rhinosinusitis involving the orbits or intracranial compartment. Air-fluid levels within the sinuses indicate acute or acute-on-chronic inflammation and increased density of intra-orbital fat characterizes orbital cellulitis (9). CT accurately depicts the orbital and extra-cranial complications, e.g. subperiosteal collection, frontal soft tissue abscess (Pott's puffy tumor); however, contrast-enhanced MRI is superior in the delineation of intracranial spread of infection (9,12). There may be little accompanying erosion of the ASB but retrograde thrombophlebitis through valveless diploic veins can lead to epidural and subdural empyemas, cerebritis and intracerebral abscess formation (Figs. 4 and 5) (9,13).

High-density secretions within the paranasal sinuses on unenhanced CT can be indicative of inspissated secretions but are also encountered in cases of fungal colonization (12). Chronic fungal disease can be markedly low signal on T2W imaging, the ''pseudo-aerated'' sinus sign; therefore, to prevent this potential pitfall, correlation must be made with the post-contrast T1W sequence and any preceding CT imaging. Assessment of

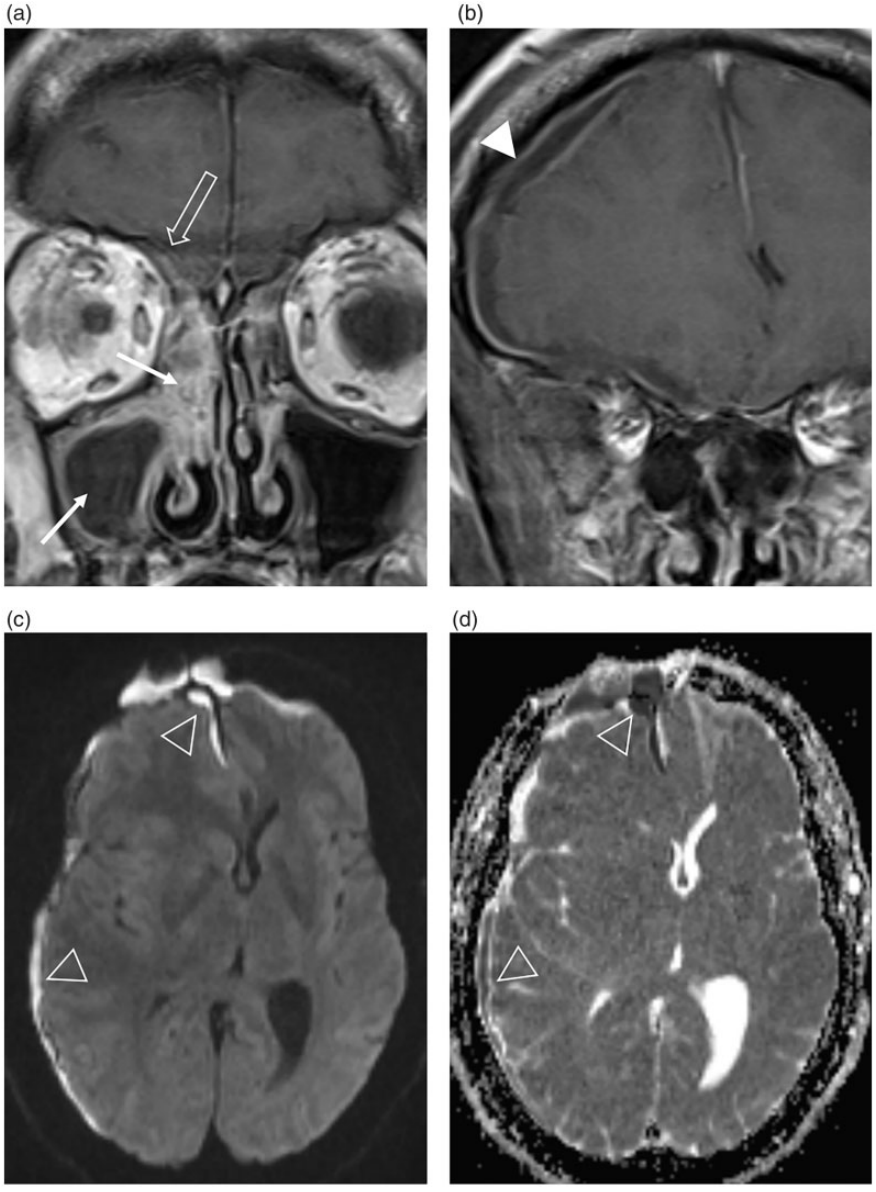

Fig. 4. Acute bacterial sinusitis complicated by an intracranial subdural empyema in a male patient presenting to A&E with a headache. (a, b) The coronal post-contrast T1W MR images demonstrate peripheral enhancement of a fluid-filled right maxillary antrum and soft tissue enhancement within the right sinonasal cavity (arrows), which extends to involve the ASB (open arrow). There is a rim-enhancing intracranial subdural collection (arrowhead) causing mass effect and midline shift. (c) The axial B1000 image and (d) corresponding ADC map demonstrate the restricted diffusion of an empyema (open arrowheads).

surrounding fat planes for inflammatory stranding can be the only finding to portend a potentially fatal invasive fungal sinusitis, usually encountered in immunocompromised patients, which can progress rapidly to involve the orbit and brain (Fig. 5) (2,9,12).

An inverted papilloma (IP) is a rare neoplasm derived from Schneiderian epithelium lining the nose and paranasal sinuses, accounting for 0.4–4% of sinonasal tumors (14). This should be suspected in cases of unilateral sinus obstruction and endoscopic evaluation suggested. The presence of focal hyperostosis on CT can predict the site of sinonasal IP attachment, which should be included in the surgical resection otherwise there is a greater risk of local recurrence (2,9). Complimentary MRI will not only aid in discriminating tumors from retained secretions but can depict the IP's distinctive convoluted cerebriform pattern of alternating hypo- and hyper-intense bands on T2W and contrast-enhanced T1W imaging (2,15). Malignant transformation of an IP can occur in approximately 10% and is associated with a destructive pattern of bone erosion, which involves the ASB in rare cases (Fig. 6) (2,16).

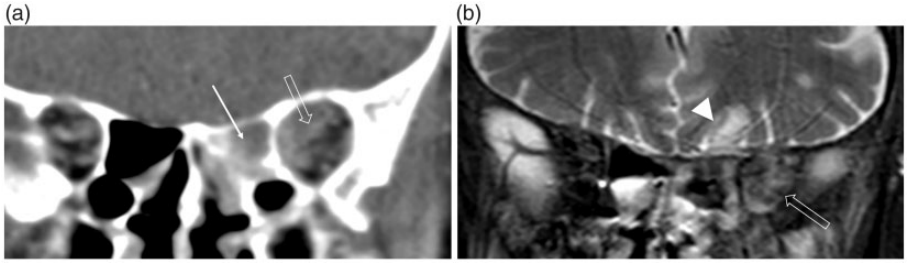

Fig. 5. Invasive fungal sinusitis in an immunocompromised patient. (a) The unenhanced coronal CT demonstrates opacification within the left posterior ethmoid sinus (arrow) and extension into the adjacent left orbital apex, obscuring normal intra- and extraconal fat (open arrow). (b) The coronal T2W fat-saturated sequence again demonstrates the inflammatory change within the left orbit (open arrow) but also demonstrates inferior frontal lobe edema (arrowhead) consistent with cerebritis secondary to intracranial spread of infection. Movement artefact in (b) is due to the poor clinical state of the patient at the time of scanning.

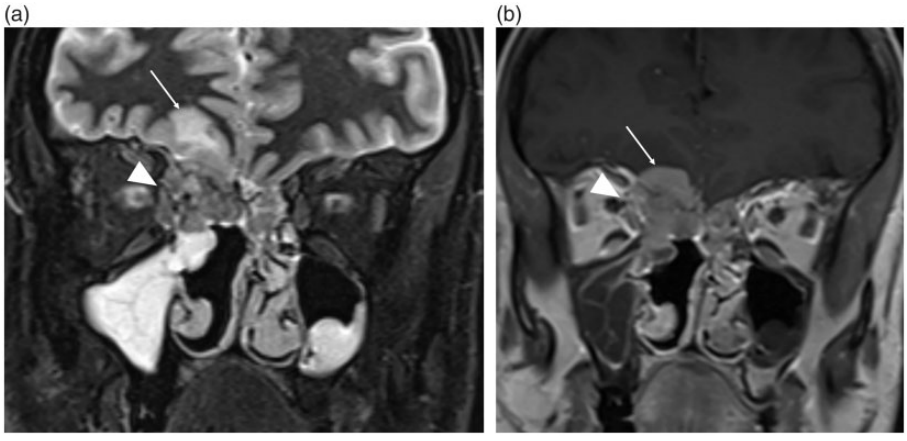

Fig. 6. Malignant degeneration in a recurrent inverted papilloma (IP) with intracranial and orbital invasion (T4b). These (a) coronal STIR and (b) T1 post-gadolinium images demonstrate an infiltrative enhancing soft tissue mass within both superior nasal cavities, larger in the right. Enhancing tumor with associated T2-dependent edema (arrows) within the right inferior frontal lobe indicates direct intracranial invasion through the ASB. The tumor also invades through the right lamina papyracea and is involving the superior oblique and medial rectus muscles (arrowhead). Post-surgical changes are present within the right nasal cavity (not labelled).

Table 1. Distinguishing features of sinonasal malignancies in relation to the ASB.

Malignancy	Distinguishing features
SCC	Usually arise from the maxillary antrum and are often advanced at presentation (Fig. 8) (5,10)
- Commonest sinonasal malignancy: 60–80% (4,19)	
- IPs can undergo unpredictable malignant degeneration to SCC in 5–15% of cases (15,16)	Invasive lesion at the site of a previously resected IP (Fig. 6)
Adenocarcinoma (non-salivary intestinal-type)	Associated with occupational exposure to wood and leather dust (10,20)
- Account for approximately 10–20% (10,20)	
- Age $\geq$ 75 years and black race are independent poor prognostic features (20)	More common within the ethmoid sinuses (2,5,20)
ACC	T2W prolongation and high propensity for perineural invasion (2,4,19)
- Commonest minor salivary gland tumor	
Sinonasal lymphoma	Variable; can be indolent and slow-growing over years or present as a rapidly enlarging mass
- Commonest extranodal lymphoma in the Asian population (usually T cell variant)	Destructive midline nasal mass, including septal perforation is commonly seen in the T cell variant

(continued)

Table 1. Continued.

Malignancy	Distinguishing features
- Rare in the Western population (more often B cell subtype) (4,21)	- may be indistinguishable from granulomatosis with polyangiitis (4,21) The B cell variant is typically a bulky homogeneous soft tissue mass involving the paranasal sinuses - may be high attenuation on CT and demonstrate restricted diffusion on DWI due to its high cellularity (2,4)
SUC and neuroendocrine carcinoma - Poor prognosis and reportedly refractory to most radical therapies when involving the skull base (10,22)	Indistinguishable from SCC; rapidly enlarging mass with aggressive features and commonly involves the ASB (10) Diagnosis often made at surgical resection due to overlapping morphological and immunohistological features with olfactory neuroblastomas (22)
Malignant melanoma	Commonly present with epistaxis and often arise from the nasal septum (2,10,19) High signal on T1WI due to melanin or hemorrhage; intense contrast enhancement (4) Can directly invade the ASB or spread by perineural invasion (2,5,23) Lymph node metastases in 40% (2)
Sinonasal sarcoma - Chondrosarcoma is the commonest variant (19)	Chondroid matrix calcification and internal enhancing septations
Olfactory neuroblastoma (ONB)/ esthesioneuroblastoma (Fig. 9) - Rare neural crest tumor arising from olfactory mucosa - Good survival rate following surgical resection (4)	Arise within the superior nasal cavity and commonly extend intracranially via the ASB (4,24) Solid polypoid mass; slightly hyperdense on CT; intense contrast enhancement (4) Cysts at the brain–tumor interface (2,10)

ASB, anterior skull base; SCC, squamous cell carcinoma; IP, inverted papilloma; ACC, adenoid cystic carcinoma; SUC, sinonasal undifferentiated carcinoma.

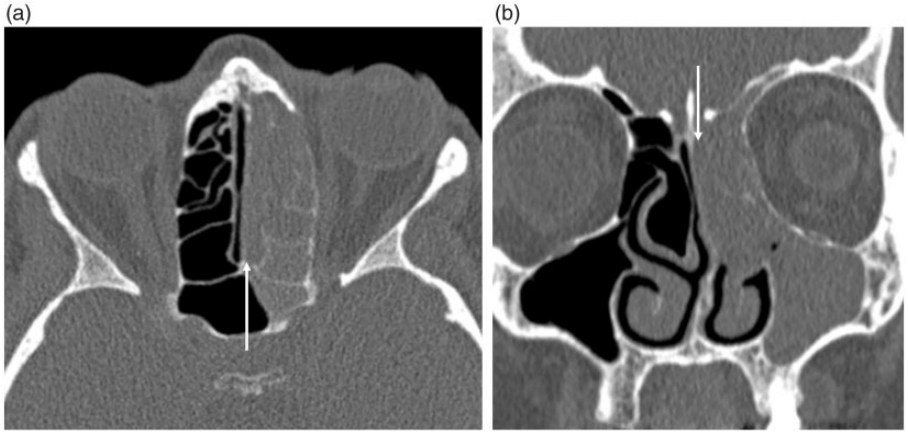

Fig. 7. Unilateral sinus opacification due to an underlying olfactory neuroblastoma (ONB). These unenhanced (a) axial and (b) coronal CT images demonstrate complete opacification of the left olfactory recess (arrows), paranasal sinuses, and middle meatus. Note the absence of mucosal thickening on the right, making rhinosinusitis less likely. This imaging finding should prompt further evaluation by direct inspection and MRI. The causative tumor, which was proven to be an olfactory neuroblastoma following biopsy, is depicted in Fig. 9.

An olfactory (or subfrontal) schwannoma is a rare benign nerve sheath tumor, closely associated with the olfactory fossa. They are postulated to arise from the fila olfactoria within the superior nasal cavity but may also originate from meningeal branches of the trigeminal nerve and anterior ethmoidal nerves (4,10,17,18). Most demonstrate hyperintense signal on T2W MRI and have variable enhancement patterns. They can

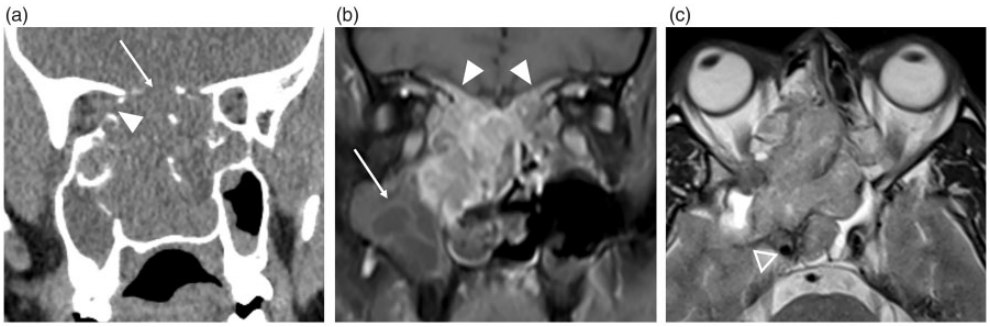

Fig. 8. Sinonasal SCC with ASB invasion and intracranial extension (T4b). (a) The coronal CT demonstrates a large sinonasal soft tissue mass which has destroyed surrounding bone within the nasal cavity, the ASB (arrow) and lamina papyracea (arrowhead). (b) The coronal T1 fat-saturated contrast-enhanced image demonstrates avid and heterogeneous enhancement of the tumor and clearly delineates that opacification of the right maxillary antrum is due to retained secretions (arrow). Enhancing tumor is seen infiltrating both sides of the ASB (arrowheads), replacing the normal low signal of cortical bone. No nodular dural enhancement was present; however, the (c) axial T2W imaging demonstrates extension posteriorly into the right middle cranial fossa and right cavernous sinus, abutting the right cavernous internal carotid artery (open arrowhead).

Fig. 9. Olfactory neuroblastoma in a female patient with a 1-year history of left rhinorrhea. A preceding CT (Fig. 7) prompted further investigation with MRI. This coronal T2W image demonstrates a smoothly marginated intermediate signal intensity mass filling the left superior nasal cavity and middle meatus. This narrows towards the ASB and has remodeled the surrounding bones – the perpendicular plate of the nasal septum is deviated to the right (arrowhead). The left olfactory bulb is indistinct with loss of normal surrounding CSF signal (open arrow), and there is possible disruption of the low signal cortex of the ASB, raising suspicion for intracranial extension. There is secondary obstruction of the left maxillary antrum, containing T2-hyperintense secretions (arrow). Given the location of the mass, an esthesioneuroblastoma must be considered however other differentials would include a nasal polyp, sinonasal SCC, and non-Hodgkin lymphoma. Histopathology from the left nasal cavity demonstrated neoplastic cells strongly positive for CD56 and synaptophysin in keeping with an olfactory neuroblastoma.

extend across the ASB in approximately 20% of cases, therefore mimicking an olfactory groove meningioma or neuroblastoma (4,10,17,18).

Malignant neoplasms

Primary sinonasal cancers account for 3% of all head and neck malignancies and all have the potential to invade the ASB (19). It is usually not possible to distinguish between histological subtypes on imaging and biopsy is required for definitive confirmation; however, there are some with more specific imaging features (Table 1). Malignant orbital tumors affecting the ASB are less common but include lymphoma, rhabdomyosarcoma, metastases, and malignant salivary gland lesions arising within the lacrimal gland (4).

An underlying neoplasm should be suspected in any patient not responding to treatment of rhinosinusitis or those with unilateral sinus opacification (Fig. 7). In general, primary sinonasal neoplasms are hypointense to intermediate signal on T1W imaging, intermediate to hyperintense on T2W imaging, and demonstrate heterogeneous enhancement depending on areas of hemorrhage and/or foci of cystic degeneration. As previously explained, the T2W and contrast-enhanced T1W sequences are particularly helpful in delineating orbital or intracranial invasion (Figs. 2, 6, 8, and 9) (9). The primary role of imaging is disease staging and reporting the extent of ASB involvement, including the presence of intracranial/orbital invasion, which is vital for any preoperative planning (endoscopic vs. neurosurgical) (25). CT and MRI can often be complementary in this assessment; however, unless there is frank bone destruction visualized on CT (Fig. 8), this imaging modality is not sensitive enough in delineating skull base or intracranial involvement and reference

must be made to contrast-enhanced MRI. The low signal T2W line representing cortical bone of the ASB or the periorbita must be scrutinized for any involvement of intermediate signal tumor (Figs. 2, 8, and 9). Sinonasal tumors are staged according to the TNM classification as T4a when there is invasion of the orbit, cribriform plate, or sphenoid, and T4b when there is intracranial extension, including extradural, dural, pial, and parenchymal invasion (this classification has not changed with the 8th edition, currently being implemented into clinical practice) (2,26). Novel endoscopic approaches to resect tumors involving the ASB, and those with extradural and dural involvement, are now possible and beneficial (27). Recurrence rates are high and MRI is the most useful modality in post-treatment follow-up, with the DWI sequence being particularly valuable (4,6,9). Detecting residual or recurrent tumors can be challenging in the presence of surgical and radiotherapy change; therefore, these studies should be reported with reference to the pre-treatment imaging as well as the surgical histopathology (knowledge of any positive surgical margins).

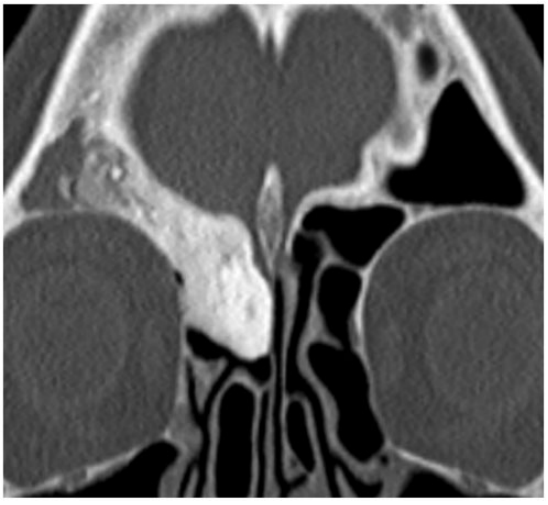

Fig. 10. Fronto-ethmoidal osteoma. Coronal CT demonstrates a well-defined ossified structure in the right fronto-ethmoidal sinus and superior nasal cavity. These can obstruct the main sinus drainage pathways; therefore, it is important to evaluate the images for any evidence of sinus expansion to suggest a mucocele.

Intrinsic ASB pathology

Osteomas are the commonest benign sinonasal bone tumor, usually present within the frontal sinus (9,19). CT is the best imaging modality in their assessment, demonstrating a well-defined, densely corticated lesion (Fig. 10). Surgical resection is not required unless they are very large or a sinus drainage pathway is obstructed. Fibrous dysplasia (FD) is a developmental disorder characterized by the replacement of normal bone with fibro-osseous tissue. It frequently involves the ASB where it can involve the orbits and optic nerve canals. The polyostotic form associated with precocious puberty is known as McCune Albright syndrome (10). FD widens the medullary cavity, with the classic sclerotic form having a diffusely ground-glass appearance on CT imaging while the pagetoid variant is a combination of sclerotic and cystic abnormality (Fig. 11) (19). MRI can be harder to interpret as the fibrous elements of the disorder can display variable T2W signal intensities and enhance heterogeneously. Aneurysmal bone cysts are uncommon bone tumors

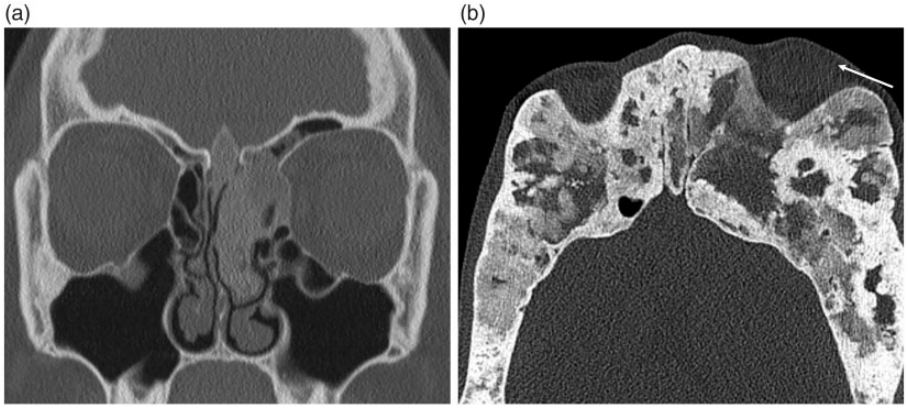

Fig. 11. Fibrous dysplasia of the ASB. (a) The classic sclerotic form is distinguished by ground-glass opacification, while (b) the pagetoid variant is a combination of sclerotic and cystic abnormality. Both forms cause expansion of the involved bone, which can lead to narrowing of the sinus drainage pathways and orbital and optic nerve complications, as demonstrated in (b) where there is involvement of the orbit causing proptosis (arrow).

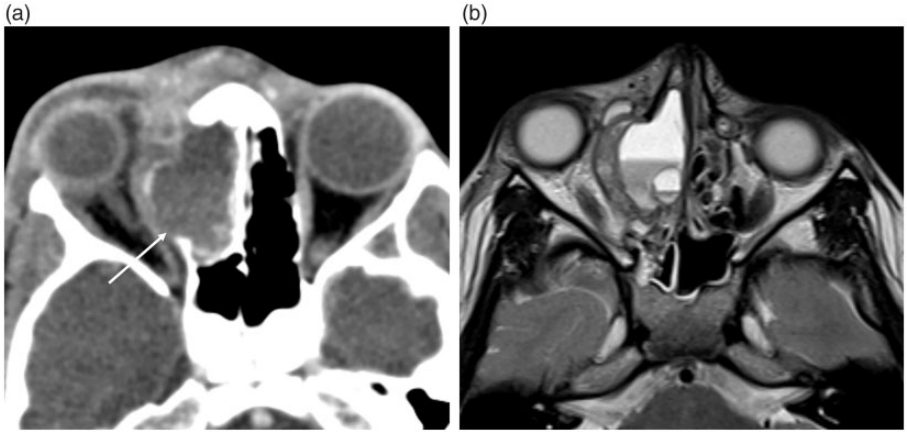

Fig. 12. Aneurysmal bone cyst in the right superior ethmoid sinus. (a) Contrast-enhanced CT depicts the bony expansion by a fluid-filled cavity and the dehiscent lamina papyracea (arrow) with lateral displacement of the right globe; and (b) the T2W MRI clearly demonstrates the characteristic fluid-fluid levels.

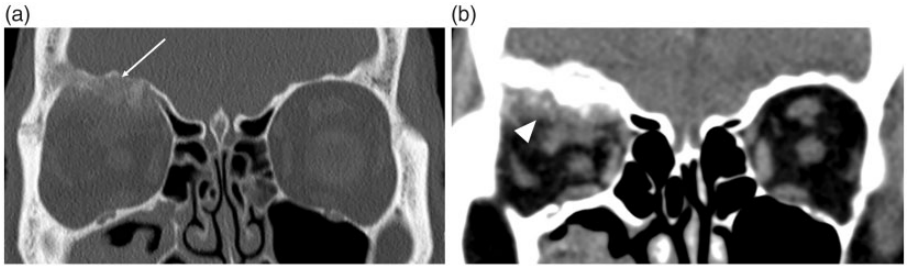

Fig. 13. ASB metastasis from prostate cancer. Coronal CT images with (a) bony and (b) soft tissue windows demonstrate an ill-defined expansile, sclerotic lesion within the orbital plate of the right frontal bone (arrow) with a soft tissue component in the superior extraconal orbit (arrowhead) causing inferior displacement of the orbital contents.

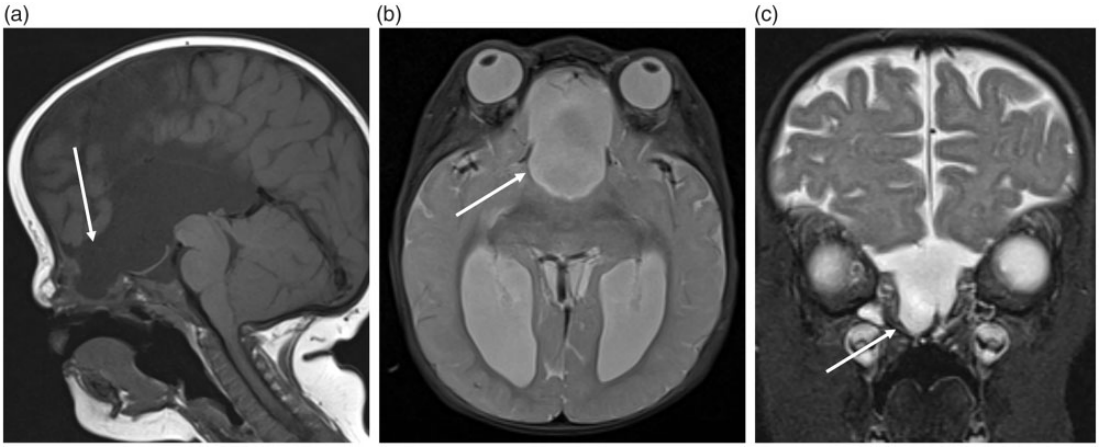

Fig. 14. Pediatric patient with a frontoethmoidal cephalocele. These (a) sagittal T1, (b) axial, and (c) coronal T2W images demonstrate a congenital cephalocele (arrows), which has developed due to failure of the prenasal space – foramen caecum to close.

with 3–6% reported to involve the skull as a whole and can occur secondarily in other primary bone tumors such as FD (2,28) CT imaging will demonstrate bony remodeling and can occasionally depict the characteristic fluid-fluid levels but these are better demonstrated on MRI (Fig. 12).

Primary ASB malignancies and metastases exhibit a destructive pattern of osseous involvement and usually

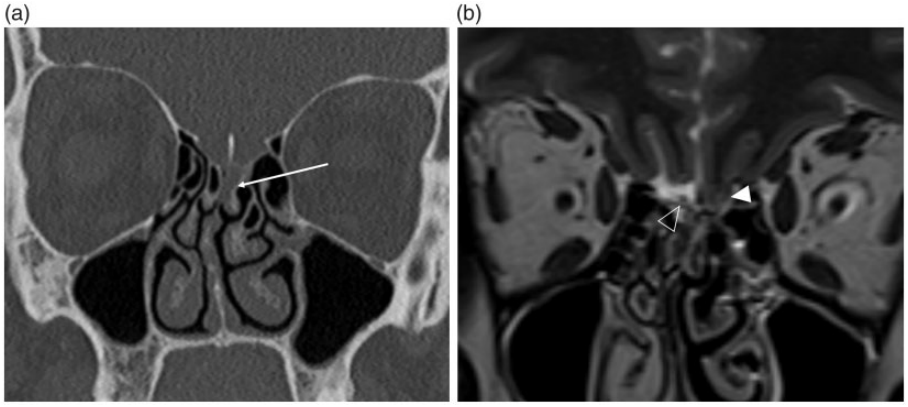

Fig. 15. Spontaneous CSF leak in an obese female presenting with rhinorrhea. (a) The coronal CT, performed as a non-contrast sinus CT study, demonstrates opacification of the left olfactory recess (arrow). Due to the nasal septal deviation to the right this would be difficult to appreciate, however in the clinical context this should be further investigated with MRI. (b) The subsequent high-resolution coronal T2W imaging depicts herniation of the left gyrus rectus into the olfactory fossa (arrowhead). The normal olfactory fossa on the right, with the olfactory bulb (open arrowhead) surrounded by CSF, is clearly visualized. There was no radiological evidence of a meningoencephalocele. The defect in the left cribriform plate was confirmed at surgery and repaired with a dural graft.

have a soft tissue component. Primary malignancies are usually sarcomas, with the commonest being osteosarcoma in adults and rhabdomyosarcoma in children (29). Metastases to the ASB are usually from breast and lung primaries but any known pre-existing malignancy should raise suspicion for this (Fig. 13) (30).

Lesions involving the ASB from above

Congenital conditions

Ossification of the ASB progresses in a constant but variable manner and is usually complete by the age of four years, with a lack of ossification thereafter suspicious for pathology, including metabolic bone disorders and dysplasias (31). Closure of the frontal and ethmoid bones around the prenasal space, which contains a strand of dura, results in formation of the foramen cecum, which can sometimes be visualized between the frontal bone and the crista galli (2,32). If regression of this dural diverticulum is incomplete, the persistent track is visualized as a widened foramen cecum and a bifid crista galli, and a spectrum of midline anomalies can occur. These include nasal gliomas (benign glial heterotopias), which do not contain CSF and have no communication with the brain, and meningoencephaloceles, which are CSF-filled and connected to the intracranial compartment (Fig. 14). Desquamation of the lining of a dermal sinus can result in a dermoid or epidermoid lesion (32). Both CT and MRI will be required to delineate the bony anatomy and differentiate between the brain parenchymal anomalies.

Kallman's syndrome describes the combination of anosmia and delayed puberty. Thin-section coronal T2W MRI will display aplasia/hypoplasia of the olfactory bulbs/nerves, absence of the olfactory sulcus, and a normal pituitary gland (33).

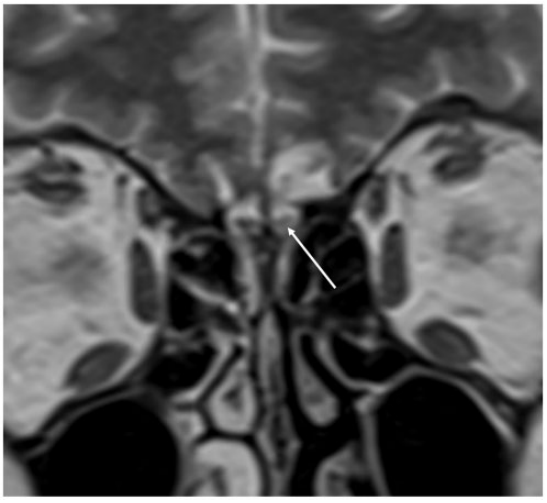

Fig. 16. Post-traumatic encephalomalacia of the inferior frontal lobe in a patient presenting with anosmia. Gliosis affecting the gyrus rectus and medial orbital gyrus with high T2-signal in the left olfactory bulb (arrow).

Acquired conditions

The cribriform plate is the commonest location for a CSF leak, which are usually secondary to trauma or iatrogenic injury (nearly 90%), although non-traumatic and spontaneous cases are well documented (34). CT cisternography, involving the intrathecal injection of contrast, is occasionally utilized but is an invasive

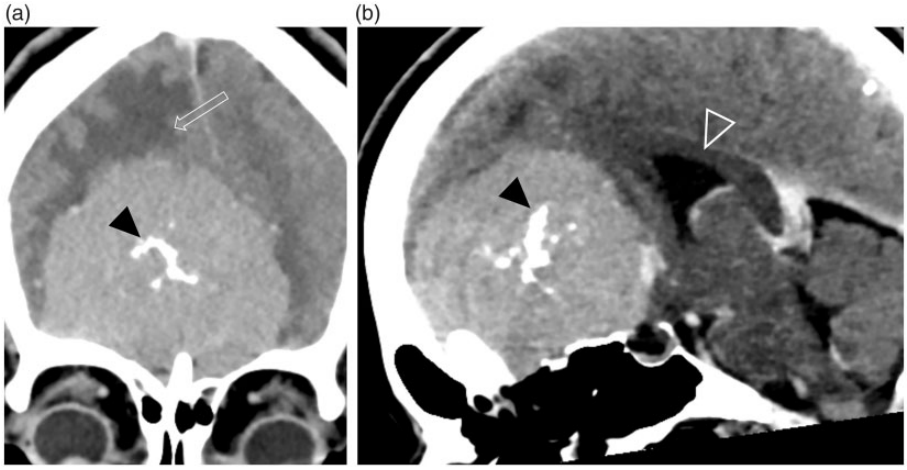

Fig. 17. Olfactory groove/planum sphenoidale meningioma in a patient presenting with headache. These (a) coronal and (b) midline sagittal contrast-enhanced CT images demonstrate a large well-defined durally based ASB lesion. The lesion enhances strongly and homogeneously, and has internal calcification (black arrowheads). Peri-lesional cerebral edema (open arrow) and posterior displacement of the corpus callosum and third ventricle (open arrowhead) indicate the significant mass effect associated with this lesion.

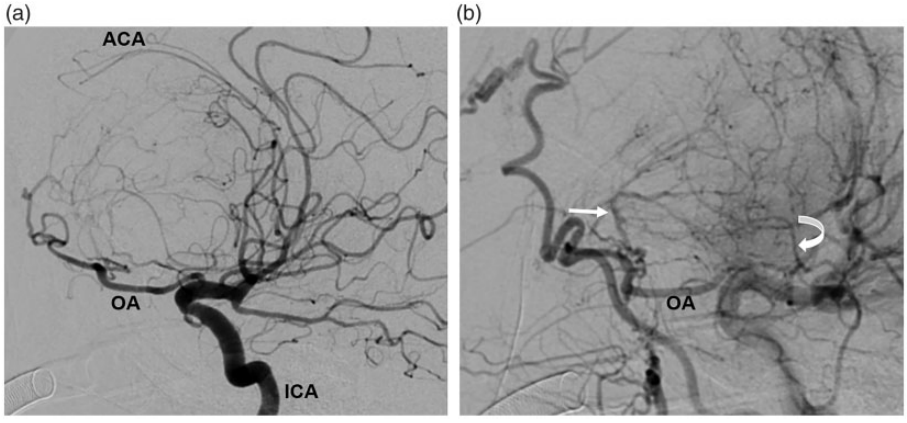

Fig. 18. Digital subtraction angiogram in the same patient as Fig. 17 before preoperative embolization. These sagittally orientated images demonstrate the anterior cerebral arteries (ACA) displaced posteriorly and draped over the top of the meningioma, indicating the degree of mass effect being exerted (a). The ophthalmic artery (OA), and on the later arterial phase image (b), the anterior (straight arrow) and posterior ethmoidal (curved arrow) arteries are hypertrophied as they are providing the blood supply to the large meningioma. ICA, internal cerebral artery.

procedure and the sensitivity relies on an active leak at the time of the procedure (34). It may be no more sensitive than unenhanced CT, which can be complemented by MRI to aid in the differentiation of a secondary meningoencephalocele. The site of a CSF leak may only be identified endoscopically following the intrathecal administration of fluorescein via lumbar puncture (30,34). A bony defect on CT should be sought but imaging may be normal or there may only be subtle suggestive findings, such as opacification of the olfactory recess (Fig. 15). In spontaneous cases, secondary imaging signs of idiopathic intracranial hypertension should be sought, e.g. empty sella, tortuous optic nerves.

Chronic complications following trauma to the ASB include encephalomalacia of the inferior frontal lobe structures, which can result in anosmia and behavioral/personality changes (Fig. 16).

Olfactory groove meningiomas are the commonest intracranial lesion affecting the ASB from above and may extend through the cribriform plate (Fig. 17) (4,35). They have the same general imaging appearances as meningiomas found elsewhere, including hyperostosis of underlying bone and the dural tail

sign (2,4,10). They derive their blood supply from the anterior and posterior ethmoidal arteries, which arise from the ophthalmic artery, and anastomose with branches of the external carotid arteries forming important intracranial to extracranial arterial connections (Fig. 18) (35). Due to their slow growth, they are often large at presentation with surgical resection usually attempted due to their mass effect, including the risk of optic neuropathy, but radiotherapy and gamma knife radiosurgery are alternative therapeutic options (35). Preoperative embolization by an interventional radiologist can help minimize blood loss and potentially reduce tumor volume in surgical cases.

Conclusion

A thorough understanding of the anatomy of the ASB and surrounding soft tissue structures will aid the radiologist in the identification and differential diagnoses of ASB pathology. While some ASB pathologies are radiologically pathognomic, many are non-specific; therefore, an accurate description of the lesion including extent and involvement of relevant structures is imperative for effective open and endoscopic surgical planning, and, when malignancy is suspected, for accurate staging.

Acknowledgements

The authors thank Kshitij Mankad, Consultant Pediatric Neuroradiologist, Great Ormond Street Hospital, for providing the congenital cephalocele case (Fig. 14) for this review.

Declaration of conflicting interests

The author(s) declared no potential conflicts of interest with respect to the research, authorship, and/or publication of this article.

Funding

The author(s) received no financial support for the research, authorship, and/or publication of this article.

References

1. Kaplanoglu H, Kaplanoglu V, Dilli A, et al. An analysis of the anatomic variations of the paranasal sinuses and ethmoid roof using computed tomography. Eurasian J Med 2013;45:115–125.
2. Iida E, Anzai Y. Sinuses and anterior skull base and relevant anatomic variations. Radiol Clin N Am 2017;55: 31–52.
3. Hingwala D, Chatterjee S, Kesavadas C, et al. Applications of 3D CISS sequence for problem solving in neuroimaging. Indian J Radiol Imaging 2011;21:90–97.
4. Borges A. Skull base tumours part I: imaging technique, anatomy and anterior skull base tumours. Eur J Radiol 2008;66:338–347.
5. Raghavan P, Phillips CD. Magnetic resonance imaging of sinonasal malignancies. Top Magn Reson Imaging 2007; 18:259–267.
6. Theony HC, De Keyzer F, King AD. Diffusion-weighted MR imaging in the head and neck. Radiology 2012;263: 19–32.
7. Newton JR, Ah-See KW. A review of nasal polyposis. Ther Clin Risk Manag 2008;4:507–512.
8. Har-El G, Todor R. Endoscopic craniofacial approach for intracranial polyposis: the ''blue-sky technique''. Skull base 2003;13:235–239.
9. Maroldi R, Ravanelli M, Borghesi A, et al. Paranasal sinus imaging. Eur J Radiol 2008;66:372–386.
10. Parmar H, Gujar S, Shah G, et al. Imaging of the anterior skull base. Neuroimaging Clin N Am 2009;19:427–439.
11. Lee JT, Brunworth J, Thompson LDR. Intracranial mucocele formation in the context of longstanding chronic rhinosinusitis: a clinicopathologic series and literature review. Allergy Rhinol (Providence) 2013;4: e166–e175.
12. Capps EF, Kinsella JJ, Gupta M, et al. Emergency imaging assessment of acute, nontraumatic conditions of the head and neck. Radiographics 2010;30:1335–1352.
13. Giannoni CM, Stewart MG, Alford EL. Intracranial complications of sinusitis. Laryngoscope 1997;107: 863–867.
14. Chawla A, Shenoy J, Chokkappan K, et al. Imaging features of sinonasal inverted papilloma: a pictorial review. Curr Probl Diagn Radiol 2016;45:347–353.
15. Jeon TY, Kim H-J, Chung S-K, et al. Sinonasal inverted papilloma: value of convoluted cerebriform pattern on MR imaging. Am J Neuroradiol 2008;29:1556–1560.
16. Wright EJ, Chernichenko N, Judson BL. Benign inverted papilloma with intracranial extension: prognostic factors and outcomes. Skull Base Rep 2011;1:145–150.
17. Figueriredo EG, Soga Y, Amorim RL, et al. The puzzling olfactory groove schwannoma: a systematic review. Skull base 2011;21:31–36.
18. Sunaryo PL, Svider PF, Husain Q, et al. Schwannomas of the sinonasal tract and anterior skull base: a systematic review of 94 cases. Am J Rhinol Allergy 2014;28:39–49.
19. EggesbØ HB. Imaging of sinonasal tumours. Cancer Imaging 2012;12:136–152.
20. Chen MM, Roman SA, Sosa JA, et al. Predictors of survival in sinonasal adenocarcinoma. J Neurol Surg B Skull Base 2015;76:208–213.
21. Borges A, Fink J, Villablanca P, et al. Midline destructive lesions of the sinonasal tract: simplified terminology based on histopathologic criteria. Am J Neuroradiol 2000;21:331–336.
22. Bell D, Hanna EY, Weber RS. Neuroendocrine neoplasms of the sinonasal region. Head Neck 2016; 38(Suppl. 1):E2259–E2266.
23. Chang PC, Fischbein NJ, McCalmont TH. Perineural spread of malignant melanoma of the head and neck: clinical and imaging features. Am J Neuroradiol 2004; 25:5–11.
24. Dublin AB, Bobinski M. Imaging characteristics of olfactory neuroblastoma (esthesioneuroblastoma). J Neurol Surg B 2016;77:1–5.

25. Gassner HG, Schwan F, Schebesch K-M. Minimally invasive surgery of the anterior skull base: transorbital approaches. GMS Curr Top Otorhinolaryngol Head Neck Surg 2016;14:Doc03.
26. Deschler DG, Moore MG, Smith RV, editors. Quick reference guide to TNM staging of head and neck cancer and neck dissection classification. 4th ed. Alexandria, VA: American Academy of Otolaryngology-Head and Neck Surgery Foundation, 2014. Available at: www.entnet.org/sites/default/files/ChapterTwoFINAL.pdf (accessed on 26 March 2017).
27. Schmalfuss IM. Imaging of endoscopic approaches to the anterior and central skull base. Radiology 2018;73: 94–105.
28. Hnenny L, Roundy N, Zherebitskiy V, et al. Giant aneurysmal bone cyst of the anterior cranial fossa and paranasal sinuses presenting in pregnancy: case report and literature review. J Neurol Surg Rep 2015;76:e216–e221.
29. Gil Z, Patel SG, Singh B, et al. Analysis of prognostic factors in 146 patients with anterior skull base sarcoma: an international collaborative study. Cancer 2007;110: 1033–1041.
30. Zacharia BE, Romero FR, Rapoport SK, et al. Endoscopic endonasal management of metastatic lesions of the anterior skull base: case series and literature review. World Neurosurg 2015;84:1267–1277.
31. Hughes DC, Kaduthodil MJ, Connolly DJ, et al. Dimensions and ossification of the normal anterior cranial fossa in children. Am J Neuroradiol 2010;31: 1268–1272.
32. Naidich TP, Blaser SI, Lien RJ, et al. Embryology and congenital lesions of the midface. In: Gaertner R, Barnes L (eds) *Head and Neck Imaging Volume 1*, 5th edn. St Louis, MO: Mosby, Inc., 2011, pp.32–55.
33. Harnsberger HR. The upper cranial nerves. In: Gay SM (ed.) *Handbook of Head and Neck Imaging*, 2nd edn. St Louis, MO: Mosby, Inc., 1995, p.464.
34. Lloyd KM, DelGaudio JM, Hudgins PA. Imaging of skull base cerebrospinal fluid leaks in adults. Radiology 2008;248:725–736.
35. Adappa ND, Lee JYK, Chiu AG. Olfactory groove meningioma. Otolaryngol Clin North Am 2011;44: 965–980.